Bull. Chem. Soc. Ethiop. **2026**, 40(1), 105-118.
DOI: https://dx.doi.org/10.4314/bcse.v40i1.9

ISSN 1011-3924
Printed in Ethiopia
Online ISSN 1726-801X

SOLVENT FREE SYNTHESIS, COMPUTATIONAL STUDIES AND IN-SILICO ADMET ANALYSIS OF SOME 3H SPIRO[1,3-BENZOTHIAZOLE –DERIVATIVES]

Felix Odame[1]*, Tatenda Madanhire[2], Anthony Selorm Kwesi Amable[1], Frempong Acheampong[1], Eric Hosten[3]

[1]Department of Basic Sciences, University of Health and Allied Sciences, PMB 31, Ho, Ghana
[2]Department of Chemistry, University of South Africa, Private Bag X6, Florida, Roodepoort, Johannesburg, 1710, Gauteng, South Africa
[3]Department of Chemistry, Nelson Mandela University, P.O. Box 77000, Gqeberha 6031, South Africa

(Received November 21, 2024; Revised June 2, 2025; Accepted September 3, 2025)

ABSTRACT. The synthesis of three spiro compounds has been achieved by a solvent-free method, and the compounds have been fully characterized. The crystal X-ray structure of 3H spiro[1,3-benzothiazole-2,1'-cyclohexane] (1) has been presented. Compound 1 crystallizes in the Orthorhombic space group *Pna21* with four (4) molecules in the unit cell characterized by unit cell parameters a = 7.7154(5) Å, b = 17.015(1) Å, c = 8.0771(5) Å, α = β= γ = 90°. The experimental bond lengths and bond angles have been compared with DFT-computed results. The Hirshfeld surface analysis of compound 1 showed that H-H interaction accounted for 68.9% of the overall crystal packing, the C-H (18.5%), S-H (9.6%), and N-H (3.0%). The *in-silico* ADMET carried out on the compounds showed that the compounds can be good candidates as potential drugs.

KEY WORDS: *In-silico* ADMET analysis, Computational, Spiro compounds, Cycloalkanone, Hirshfeld analysis

INTRODUCTION

Spiro compounds are compounds containing two rings with one shared carbon atom that is sp^3 hybridized. The compounds occur widely in nature with potential for a wide range of activities [1, 2]. Spiro compounds have been synthesized by different techniques [1-10]. They have been studied because of their versatility; they have found use as antitumor agents [3-6], anti-inflammatory agents [7-9], and anti-microbial agents [10]. Spiro-type compounds have found application as molecular hole-conduction materials [11]. Some conjugated acetylene-linked compounds containing methoxy triphenylamine terminal groups and thiophene derivatives have been accessed and used as hole-transporting materials [12]. Hole transport materials have been designed for application in quantum dot sensitized solar cells. Substituents on phenyl groups enhanced the hole transport features of these materials. When hydrogen was the only substituent, the compounds exhibited higher hole mobility than when spiro compounds were used [13-15]. The synthesis of some spiroindoles have been achieved *via* microwave irradiation. The indol-2,3-diones reacted with different heterocyclic amines to give Schiff bases, which were then converted to spiro compounds [16]. The synthesis of fluorinated spiro[3H-indole-3,20-tetrahydro-1,3-thiazine]-2,40(1H)-diones, fluorinated spiro[3H-indole-3,20-thiazolidine]-2,40 (1H)-diones was achieved by using an ionic liquid as a catalyst and initiated by microwave irradiation [17]. Microwave irradiation has been used on solvent-free systems to achieve greater yields in synthesis [18]. Shorter reaction times have been achieved by microwave irradiation in reaction systems that contain organic solvents [19]. Microwave irradiation has been used in some nanoparticle-catalysed reactions [20]. A series of spiro[(2H,3H)quinazoline-2,1`-cyclohexan]-4(1H)-one

*Corresponding author. E-mail: felixessah15@gmail.com

derivatives have been synthesized as poly-ADP ribose polymerase (PARP-1) inhibitors. Most of the compounds showed effective anti-proliferative activity against breast carcinoma cell lines and were effective against the target PARP-1 enzyme [9]. The insertion of a methylene group have been achieved in the synthesis of 3′-methylene bis(4-hydroxyquinolin-2(1H)-ones). *In silico* results showed that, the compounds have good binding affinity to the severe acute respiratory syndrome coronavirus 2 (SARS-CoV-2 main protease (Mpro) when compared with Darunavir [10]. We herein report, the Hirshfeld surface analysis, computational studies, and absorption, distribution, metabolism, excretion, and toxicity (ADMET) analysis of three 3H spiro[1,3-benzothiazole- derivatives.

MATERIALS AND METHOD

Sigma Aldrich (USA) supplied analytical-grade reagents and solvents for synthesis, including 2-Aminophenol, cyclohexanone, cycloheptanone, and cyclooctanone, while Merck Chemicals (SA) supplied ethanol, methanol, and ethyl acetate. The chemicals were employed as they were delivered, meaning they were not further purified. Using DMSO-d_6 as the solvent and tetramethylsilane as the internal standard, ^{1}H and ^{13}C-NMR spectra were captured on a Bruker Avance AV 400 MHz spectrometer running at 400 MHz for ^{1}H and 100 MHz for ^{13}C, and chemical shifts (ppm are used to express chemical changes. A Bruker Platinum ATR Spectrophotometer Tensor 27 was used to record FT-IR spectra. A Vario Elementar Microcube ELIII was used to conduct elemental analysis. A Stuart Lasec SMP30 was used to estimate melting points, and an Agilent 7890A GC System coupled to a 5975C VL-MSC with electron impact as the ionization mode and triple-axis detection was used to determine the masses. A 30 m x 0.25 mm x 0.25 µm DB-5 capillary column was installed in the GC. Helium was employed as the carrier gas at a pressure of 63.73 kPa, a flow rate of 1.63 mL.min^{-1}, and an average velocity of 30.16 cm s^{-1}.

*3H spiro[1,3-benzothiazole-2,1'-cyclohexane] (**1**)*

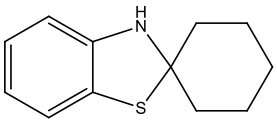

2-Aminothiophenol (0.02 mol, 2.50 g) was mixed with cyclohexanone (0.02 mol, 1.96 g) in a round-bottom flask and heated at a consistent temperature with stirring for 12 hours. The reaction mixture was allowed to cool, and 30 mL of methanol was added to dissolve it. The product was recrystallized and obtained as a light brown solid from ethanol: ethyl acetate (1:1). Yield = 84%, m.p = 93-94 °C, ^{1}H-NMR (ppm): 6.95 (d, *J* = 6.4 Hz, 1H), 6.82 (t, *J* = 6.4, 7.2 Hz, 1H), 6.54 (d, *J* = 7.2 Hz, 2H), 6.43 (s, 1H), 2.08 (m, 2H), 1.80 (m, 4H), 1.47 (m, 2H), 1.25 (m, 2H). ^{13}C-NMR (ppm): 147.6 (C-N), 125.4 (CH), 125.1 (C), 121.7 (CH), 118.4 (CH), 109.2 (CH), 80.7 (C), 41.0 (CH_2CH_2), 25.0 (CH_2), 24.0 (CH_2CH_2). IR (ν_{max}, cm^{-1}): 3329 (N–H), 2949 (C–H), 2953 (C–H), 1580 (C=C), 1456 (C–N), 1393 (C-N). Anal. calcd. for $C_{12}H_{15}NS$: C, 70.20; H, 7.36; N, 6.82; S, 15.62. Found: C, 70.15; H, 7.28; N, 6.72; S, 15.50. LRMS (*m/z*, M^+): Found for $C_{12}H_{15}NS$ = 205.32, Expected mass = 205.20. The 5-chloro-4'-ethyl-*3H*-spiro[1,3-benzothiazole-2,1'-cyclohexane] derivative has been synthesized by the reaction of 2-amino-4-chlorothiophenol (0.01 mol) and 4-ethylcyclohexanone (0.01 mol) in absolute ethanol (50 mL) under reflux on a water bath for 8 h. [21].

3H-spiro[benzo[d]thiazole-2,1'-cycloheptane] (**2**)

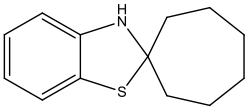

2-Aminothiophenol (0.02 mol, 2.50 g) was mixed with cycloheptanone (0.02 mol, 2.24 g) in a round-bottom flask and heated under reflux at a constant temperature for 12 hours. The reaction mixture was cooled, and 30 mL of methanol was added to dissolve it. The product was

recrystallized and obtained as a brown solid from ethanol: ethyl acetate (1:1). Yield = 71%, m.p = 92-93 °C ^{1}H-NMR (ppm): 7.01 (s, 1H), 6.95 (d, 1H, *J* = 7.6 Hz), 6.87 (t, 1H, *J* = 7.6 Hz), 6.57 (m, 1H), 2.37 (m, 2H), 2.18 (m, 2H), 1.89 (m, 2H), 1.76 (m, 2H), 1.66 (m, 2H), 1.39 (m, 2H) . ^{13}C-NMR (ppm): 149.6 (C=N), 126.2 (Ph–H), 122.9 (C), 122.2 (Ph–H), 118.9 (Ph–H), 109.2 (Ph–H), 82.8 (C), 38.3 (CH_2), 38.0 (CH_2), 29.3 CH_2), 26.3 (CH_2), 25.6 CH_2). IR (νmax, cm^{-1}): 3322 (N–H), 3224 (N–H), 2947 (C–H), 1668 (C=C), 1602 (C=C), 1525 (C=C), 1300 (C–O). Anal.calcd. for $C_{13}H_{17}NS$: C, 71.18; H, 7.81; N, 6.39; S, 14.62. Found: C, 71.11; H, 7.73; N, 6.32; S, 14.53. LRMS (m/z, M^+): Found for $C_{13}H_{17}NS$ = 219.21, Expected mass =219.35.

*3H-spiro[benzo[d]thiazole-2,1'-cyclooctan] (**3**)*

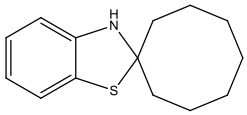

2-Aminothiophenol (0.02 mol, 2.50 g) was mixed with cyclooctanone (0.02 mol, 2.52 g) and heated under reflux at a constant temperature for 12 hours. The product was recrystallized and obtained as a brown solid from ethanol: ethyl acetate (1:1). Yield = 68%, m.p = 89-91 °C, ^{1}H NMR (ppm): 7.01 (br, 1H), 6.95 (d, *J* = 7.2 Hz, 1H), 6.87 (t, *J* = 72, 7.6 Hz, 1H), 6.57 (t, 2H), 2.826 (t, *J* = 11.6Hz, 2H), 2.37 (m, 2H), 2.18 (t, *J* =10-14.4 Hz, 2H), 1.91 (m, 2H), 1.77 (m, 2H), 1.652 (m, 2H), 1.45 (m, 2H). ^{13}C-NMR (ppm): 149.5 (C=N), 126.3 (Ph–H), 122.9 (C), 121.8 (Ph–H), 119.0 (Ph–H), 109.2 (Ph–H), 82.8 (C), 38.4 (CH_2), 37.8 (CH_2), 29.5 (CH_2), 26.5 (CH_2), 25.6 (CH_2). IR (νmax, cm^{-1}): 3287 (N–H), 2933 (C–H), 2857 (C-H), 1702 (C=C), 1579 (C=C), 1463 (C-N). Anal. calcd. for $C_{14}H_{19}NS$: C, 72.05; H, 8.21; N, 6.00; S, 13.74. Found: C, 71.96; H, 8.13; N, 5.91; S, 13.65. LRMS (m/z, M^+): Found for $C_{14}H_{19}NS$ = 233.29, Expected mass = 233.37.

X-ray crystal structure determination

An X-ray diffraction study of compound **1** was carried out at 200 K using monochromated Mo Kα radiation (λ = 0.71073 Å) with a Bruker Kappa Apex II diffractometer. Data collection for cell refinement and data reduction was done using APEXII and SAINT [22]. Structure determination was done directly using SHELXT-2018/2 [23] and refined by least-squares procedures with SHELXL-2018/3 [24], whilst SHELXLE [25], served as a graphical user interface. The carbon-bound H atoms were incorporated in the refinement in the riding model approximation, with Uiso (H) set to 1.2Ueq (C), and placed at estimated positions (C–H 0.95 Å for aromatic carbon atoms and C–H 0.99 Å for methylene groups). The non-hydrogen atoms were refined anisotropically. The use of numerical techniques in SADABS [22] were employed for absorption effects and data correction. The ORTEP-3 was used to create the molecular visualizations [26] whilst mercury [27] and PLATON [28] were used for preparing the materials for publication.

Computational studies

The Gaussian 09 program was used for all computations [29]. Compound **1** was optimized at the singlet ground state in the gas phase at the density functional theory (DFT) using the 6-311g (d,p) basis set and the B3LYP, CAM-B3LYP, B3PW91, and WB97XD [30-32] functionals. Optimization and frequency computation were done to ensure that the enhanced molecular structure matched a minimum. Gaussview 6.0 [33] and Avogadro [34] were used to observe the results. The choice of basis set and functionals was based on previous studies [30-32].

Hirshfeld surface analysis

An effective method for illustrating interactions in molecular crystals is Hirshfeld surface analysis. A computer program called Crystal Explorer 3.1 uses the computed Hirshfeld surfaces

of molecules inside a crystal structure to ascertain the intermolecular interactions between specific molecules or for the entire crystal structure. A quantitative method for examining the intermolecular interactions between the molecules in a crystal structure is Hirshfeld surface analysis. Additionally, it provides information about their crystal packing behavior. The software Crystal Explorer 3.1 was used to map fingerprint plots and Hirshfeld surfaces [35]. Using a static color scale and high surface resolution, the normalized contact distance (*dnorm*) was used to show the analysis. The van der Waals radius of the atom is given by *rvdw*, *di* is the corresponding distance to the nearest nucleus inside the surface, and *de* is the distance from the Hirshfeld surface to the nearest nucleus outside the surface [36]. The *dnorm* parameter displays a red-white-blue color surface. The shape index gives a qualitative difference in the shapes of surfaces. It is helpful in detecting subtle differences in areas that show as relatively flat [37]. A measure of the shape of the surface area of the molecule is its curvedness [38].

HOMO LUMO analysis

DFT has been used to assess the energy gaps for the lowest unoccupied molecular orbitals (LUMOs) and highest occupied molecular orbitals (HOMOs). The frontier orbitals help explain a variety of reactions in conjugated systems and forecast the most reactive position in π-electron systems [39]. Due to a considerable amount of intramolecular charge transfer from the end capping electron-donor groups *via* a π-conjugated path, the conjugated molecules have a small highest occupied molecular orbital-lowest unoccupied molecular orbital gap (HOMO and LUMO separation) [40]. The primary orbitals that determine a species' chemical stability are the HOMO and LUMO [41]. The ability to give an electron is represented by the HOMO, and the ability to accept an electron is represented by the LUMO. Whereas the LUMO's energy is correlated with electron affinity, the HOMO's energy is directly tied to the ionization potential. The stability or reactivity of molecules is determined by the energy gap, the difference between the HOMO and LUMO orbitals [42]. Since the energy gap is a measure of electron conductivity, it is a crucial factor in establishing the electrical transport characteristics of molecules [43]. The hardness of a molecule also corresponds to the gap between the HOMO and LUMO orbitals [44].

Basis of ADMET Analysis

ADMET Lab 2.0 was used to calculate several properties such as bioavailability, blood-brain barrier penetration, plasma-protein binding, and metabolism. Although there are many steps involved in drug discovery and design, adsorption, metabolism, excretion, and toxicity assessments are all highly useful [45]. While safety and efficacy are some of the challenges in the creation of novel pharmaceuticals, computational methods have emerged as a very useful addition to the discovery of new drugs [46]. The compounds' ADMET (absorption, distribution, metabolism, excretion, and toxicity) characteristics are crucial to the drug-discovery process. A bioactive agent with good ADMET capabilities is a good candidate to be developed into a drug; this is greatly enhanced when the chemical satisfies the drug-likeness requirements [47]. The Lipinski rule of five is a useful criterion for distinguishing between various substances' characteristics, prospective uses as medications, and possible routes of administration. Molecular weight (MW) < 500, octanol/water partition coefficient (A log P) ≤ 5, the number of hydrogen bond donors (HBDs) ≤ 5, and the number of hydrogen bond acceptors (HBAs) ≤ 10 were the five evaluation criteria [48]. If a compound falls short or violates two or more of the criteria, then it would not be orally active.

RESULTS AND DISCUSSION

*Crystal structure of compound **1***

The compounds were synthesized by a solvent-free heating of 2-aminothiophenol and the respective cycloalkanone for 12 hours. It was recrystallized from ethanol:diethyl ether (1:1) as light brown or brown crystals. Scheme 1 gives the synthetic scheme for 3H-spiro[1,3-benzothiazole derivatives.

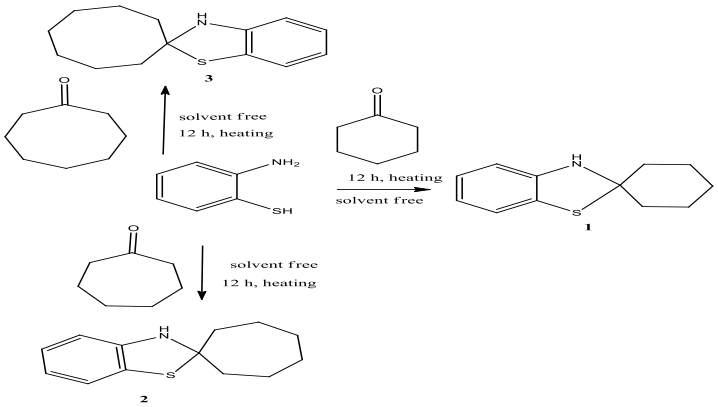

Scheme 1. Synthetic scheme for 3*H* spiro[1,3-benzothiazole derivatives.

A series of spirocyclohexane-1,4′-pyrazolothiazepinones has been accessed by one-pot multicomponent cyclocondensation reactions between 5-amino-1-arylpyrazoles, cyclohexanone, and mercaptoacetic acid. The scope of reaction and mechanism of the reaction were studied [1]. Some 2,3-dihydronaphtho[2,3-d][1,3]thiazole-4,9-diones and 2,3-dihydroanthra[2,3-d][1,3]thiazole-4,11-diones have been synthesized by the reaction of 2-(methylamino)naphthoquinones and anthracene-1,4-diones with S_2Cl_2 and 1,4-diazabicyclo[2.2.2]octane (DABCO). 3H-Spiro(thiazol-2,1'-cyclohexanes) underwent a new ring contraction and fusion reaction, resulting in the formation of tetrahydroindoles. The reaction was explored for other substrates [2]. The synthesis of spiro[indene-2,3′-indeno[2′,1′:5,6]pyrano[2,3- b]pyridines] has been achieved by the reaction of *N*-arylaldimines with two moles of 2-arylidene-1,3-indanediones in dry acetonitrile. The reaction proceeded in the absence of a catalyst, and the product was obtained in moderate yield [3]. The formation of 5-chloro-4'-ethyl-3H-spiro[1,3-benzothiazole-2,1'-cyclohexane] has been achieved by the reaction of 2-amino-4-chlorothiophenol and 4-ethylcyclohexanone in absolute ethanol [4]. 3-Aryl benzo[d]thiazole-2(3H)-imines have been synthesized by the reaction between diazonium salt and different thioureas [5]. Different spiro[benzo[b]thiophene-2(3H),1'-cyclopropan]-3-one derivatives have been synthesized by a domino reaction between thioaurones and sulfur ylides [6]. The synthesis of triphenylphosphanylidene spiro[cyclopentane-1,3′-indoline] and spiro[cyclopent [2]-ene-1,3′-indoline] has been achieved by the reaction between triphenylphosphine, but-2-ynedioate, and isatylidene malononitrile (ethyl cyanoacetate) [7]. 2,3-Dihydronaphtho[2,3-d][1,3]thiazole-4,9-diones and 2,3-dihydroanthra[2,3-d][1,3] thiazole -4,11-diones have been accessed by the reaction of *N*-substituted 2-(methylamino) naphthoquinones and -anthracene-1,4-diones in the presence of S_2Cl_2 [8].

The crystallographic data, selected bond lengths, and bond angles for the crystal structure of compound 1 are provided in Tables 1 and S4. The ORTEP diagram for compound **1** is presented

in Figure 1. The compound crystallizes in the orthorhombic space group *Pna21* with four (4) molecules in the unit cell characterized by unit cell parameters a = 7.7154(5) Å, b = 17.015(1) Å, c = 8.0771(5) Á. Table S4 gives the summary of theoretical and experimental bond lengths and bond angles for compound **1** using B3LYP, CAM-B3LYP, B3PW91 and WB97XD functionals and 6-311g basis set. The level of theory chosen has been reported in literature to give results, which are consistent with the experimental results [30-32]. The bond lengths S1-C12 and S1-C21 are 1.759(2) and 1.860(2) Å respectively which are consistent with typical C-S bonds [49-50], gave deviations between 0.019 and 0.092 Å whilst the bond distances of N1-C11 and N1-C21 are 1.388(2) and 1.475(2) Å respectively which were consistent with C-N single bonds [49-50], gave deviations between 0.026 and 0.084Å.

Table 1. Crystallographic data and structure refinement summary for compound **1**.

Property	**1**
Formula	$C_{12}H_{15}NS$
Formula weight	205.31
Crystal system	Orthorhombic
Space group	*Pna21*
a [Å]	7.7154(5)
b [Å]	17.015(1)
c [Å]	8.0771(5)
α [°]	90
β [°]	90
γ [°]	90
V [Å^3]	1060.34(11)
Z	4
D(calc) [g/cm^3]	1.286
Mu(MoKa) [/mm]	0.264
Flack x	0.021(15)
F(000)	440
Crystal size [mm]	0.56 x 0.56 x 0.56
Temperature (K)	200
Radiation [Å] MoKa	0.71073
θ Min-Max [°]	2.4, 28.3
Dataset	-9: 10; -22: 22; -10: 10
Tot., Uniq. Data, R(int)	13788, 2505, 0.019
Observed data [I > 2.0 sigma(I)]	2410
Nref,	2505
Npar	131
R	0.0237
$_wR_2$	0.0619
S	1.05
Max. and Av. Shift/Error	0.00, 0.00
Min. Resd. Dens. [e/Å^3]	-0.18,
Max. Resd. Dens. [e/Å^3]	0.18

The bond distances of C11-C12, C11-C16 and C12-C13, are 1.403(2), 1.389(2) and 1.383(2) Å which were consistent with C-C single bonds [49-50] gave deviations from 0.022 to 0.079 Å. The bond distances of C13-C14, C14-C15, C21-C26 and C21-C22, which were consistent C-C single bonds [49-50], with deviations between 0.011 and 0.072 Å. The bond angles of C12-S1-C21 and C11-N1-C21 were experimentally determined as 90.2(1) and 111.6(1)° whilst the computed values gave deviations of between 3.6 and 8..2° from the experimental values.

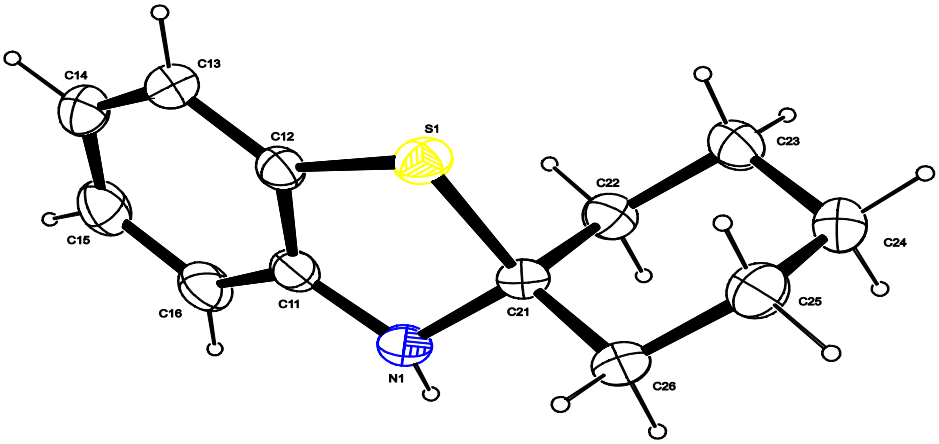

Figure 1. An ORTEP view of showing 50% probability displacement ellipsoids and atom labelling for compound **1**.

Hirshfeld surface analysis

The *dnorm* parameter displays a red-white-blue color surface. Blue spots indicate intermolecular connections that are longer than their vdW radii, whereas bright red spots indicate intermolecular contacts that are shorter. Their vdW radii add up to white patches. Bright red spots show the intermolecular contacts less than their vdW radii, while the blue spots show intermolecular contacts longer than their vdW radii. White spots are the sum of their vdW radii. Figure 2 shows the molecular Hirshfeld surfaces that were created using a standard (high) surface resolution. These surfaces include the *dnorm* surface, shape index, and curvedness of compound **1**. The *dnorm* surface was mapped on over the range of -0.1420 Å to 1.1878 Å, shape index in the range of -1.0000 Å. to 1.0000 Å and curvature in the range of -4.0000 Å to 0.4000 Å, *di* was mapped over the range 1.0108 Å to 2.4846 Å, de ranged from 1.0103 to 2.4605 Å, fragment patch was in the range 0.0000 to 13.0000 Å. Figure 2 gives the two-dimensional (2D) fingerprint plots from Hirshfeld surface analyses of compound **1**.

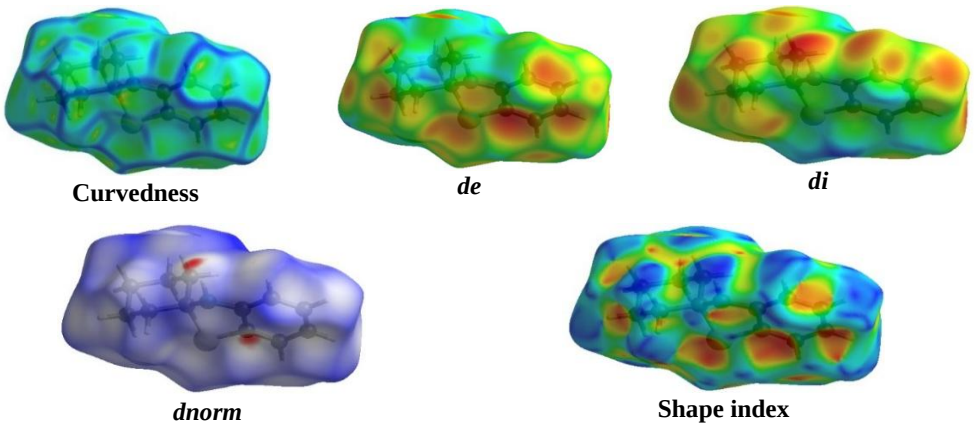

Figure 2. Hirshfeld surfaces mapped for (a) d norm surfaces, (b) shape index and (c) curvature of 3H spiro[1,3-benzothiazole-2,1'-cyclohexane] (**1**).

The H-H interaction gave a contribution of 68.9% to the overall crystal packing, the C-H (18.5%), the S-H (9.6%) and N-H (3.0%) fingerprint plots provide information about the intermolecular hydrogen bonds and the contribution of the individual elements towards the crystal packing. The electron density of the surface curves around the chemical interactions, as indicated by the curvedness. Whereas the sharp curvature area, which typically tends to divide the surface into patches and indicates connections between neighbouring molecules, corresponds to high values of curvedness, the flat areas of the surface correlate to low levels of curvedness.

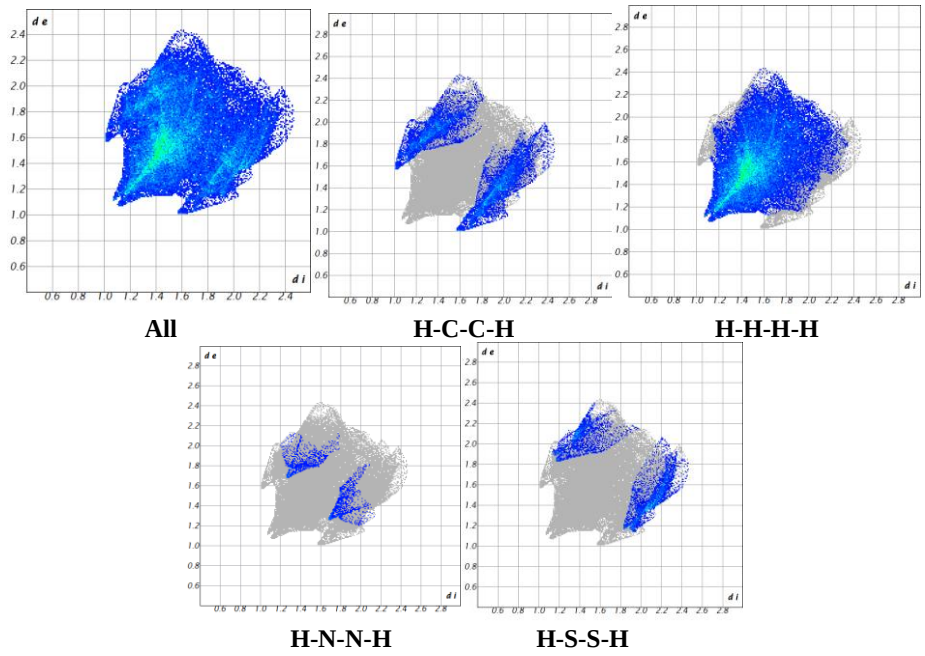

Figure 3. Relative contributions to the percentage of Hirshfeld surface area for the various intermolecular contacts in 3H spiro[1,3-benzothiazole-2,1'-cyclohexane] (**1**).

HOMO LUMO analysis

The computation of the HOMO-LUMO gaps of compound **1** gave varying gaps for the functionals and basis set used of B3LYP (0.0901), CAM-B3LYP (0.09119), B3PW91 (0.37042), and WB97XD (0.10589). Tables 3 and S4 give the HOMO –LUMO computation and the plots. The HOMO for compound **1** is distributed over the benzothiazole ring, specifically the phenyl ring and the heteroatoms (sulphur and nitrogen), with no noticeable contribution from the cyclohexyl ring. The LUMO is distributed over the benzothiazole ring with some contribution from the cyclohexyl ring. This shows that the most reactive portion of the molecule is the benzothiazole moiety, which uses the cyclohexyl ring for stabilization when attacked by a nucleophile. This means that substitution reactions and addition reactions will mostly occur on the benzothiazole ring.

Table 2. HOMO–LUMO energy levels of 3*H* spiro[1,3-benzothiazole-2,1'-cyclohexane] (**1**) using B3LYP, CAM-B3LYP, B3PW91 and WB97XD functionals and 6-311g(d,p) basis set.

Compound **1**				
Energy levels	B3LYP (eV)	CAM-B3LYP (eV)	B3PW91 (eV)	WB97XD (eV)
LUMO+4	-0.26891	-0.25941	-0.17313	-0.27971
LUMO+3	-0.32799	-0.32532	-0.18425	-0.32319
LUMO+2	-0.33345	-0.33368	-0.19936	-0.32646
LUMO+1	-0.34946	-0.35006	-0.25269	-0.34290
LUMO	-0.48682	-0.48806	-0.28058	-0.48171
HOMO	-0.57692	-0.57925	-0.65100	-0.58760
HOMO-1	-0.58142	-0.58296	-0.65656	-0.59015
HOMO-2	-0.58614	-0.58671	-0.66173	-0.59207
HOMO-3	-0.58836	-0.59010	-0.66304	-0.59538
HOMO-4	-0.62522	-0.62690	-0.70241	-0.63248
HOMO-LUMO GAP (eV)	0.0901	0.09119	0.37042	0.10589

ADMET Analysis

Table 3 gives the ADMET results for compound **1–3** (A) physicochemical properties, (B) medicinal chemistry, (C) absorption, (D) distribution, (E) metabolism, (F) excretion, (G) toxicity, (H) environmental toxicity, (I) tox21 pathway. The ADMET lab 2.0 platform was used to obtain the physicochemical properties of the compounds. Different physicochemical and pharmacokinetic properties were determined. All the compounds were donors as well as acceptors of hydrogen bonds. None of the compounds has a rotatable bond. The compounds' lower topological polar surface area values (12.030) indicated that they were less flexible than ampicillin (112.73). Compounds **1** and **2** gave a log S values greater than -4 log [mol/L] whilst compound **3** gave a log S value of -4.106 log [mol/L] with Ampicillin giving a log S of -1.564 log [mol/L]. All of the compounds showed good oral bioavailability and high gastrointestinal absorption. This indicates that the compounds all have good cell permeability and transport properties. All the compounds have a molecular weight between the suggested range of 205 to 380 g/mol. The compounds gave lipophilicity (log P) values within the permissible range of 2.3 and 5.0. The compounds showed good drug likeness, as indicated by Lipinski "Rule of Five," which includes to have log P less than or equal to 5, MW less than or equal to 500, to have number of hydrogen bond donors less than or equal to 5, and a number of hydrogen bond acceptors less than or equal to 10. The compounds complied with Lipinski's Rule of Five (RO5). The *in silico ADMET results show that the physicochemical properties of the compounds can be improved through the* introduction of new substituents.

Table 3. Molecular properties of compound **1-3** (A) physicochemical properties, (B) medicinal chemistry, (C) absorption.

A. Physicochemical properties				
Property	**1**	**2**	**3**	Ampicillin
Molecular weight	205.090	219.110	233.120	349.110
Volume	212.035	229.331	246.627	330.464
Density	0.967	0.955	0.945	1.056
NHA	1	1	1	7
NHD	1	1	1	4
NRot	0	0	0	5
NRing	3	3	3	3

MaxRing	9	9	9	7
NHet	2	2	2	8
FChar	0	0	0	0
NRing	16	17	18	17
Flexibility	0.000	0.00	0.000	0.294
Stereo Centers	0	0	0	4
TPSA	12.030	12.030	12.030	112.73
log S	-3.275	-3694	-4.106	-1.564
log P	3.522	3.916	4.351	0.899
log D	3.326	3.634	3.871	0.589

B. Medicinal chemistry				
Property	**1**	**2**	**3**	Ampicillin
QED	0.690	0.700	0.700	0.675
Synthetic accessibility score	3.181	3.120	3.070	3.527
Fsp3	0.500	0.538	0.571	0.438
MCE-18	51.333	51.800	52.182	70.304
NPscore	-0.198	-0.185	-0.173	0.742
Lipinski's rule	Yes	Yes	Yes	Yes
Pfitzer	No	No	No	Yes
GSK rule	Yes	Yes	No	Yes
Golden triangle	Yes	Yes	Yes	Yes

C. Absorption				
Property	**1**	**2**	**3**	Ampicillin
Caco-2 permeability	-4.550	-4.593	-4.625	-5.910
MDCK permeability	1.8 e-05	1.6 e-05	1.4 e-05	3.1e-0.5
Pgp inhibitor	Excellent	Excellent	Excellent	Excellent
Pgp substrate	Excellent	Excellent	Excellent	Excellent
Human intestinal absorption	Excellent	Excellent	Excellent	Excellent
Human oral bioavailability 20%	Excellent	Excellent	Excellent	Excellent
Human oral bioavailability 30%	Excellent	Excellent	Excellent	Excellent

CONCLUSIONS

Three spiro compounds have been accessed without the use of solvents; compound 1 crystallized in the orthorhombic space group *Pna21*, having four molecules in the unit cell. A comparison of the DFT calculations with experimental bond lengths and bond angles showed good agreement amongst the results. The Hirshfeld surface analysis showed that the most important interactions were the H-H interaction (68.9%), followed by the C-H (18.5%), S-H (9.6%), and N-H (3.0%). The in *in-silico* ADMET analysis showed that the compounds have the potential as future medications.

ACKNOWLEDGEMENTS

The authors would like to acknowledge the Centre for High Performance Computing in South Africa for the use of their computing resources (CHEM1261).

Supporting information

CCDC-2181454 contains the additional crystallographic data for this paper. These data can be obtained free of charge via https://www.ccdc.cam.ac.uk/ structures/, or by e-mailing data_request@ccdc.cam.ac.uk, or by contacting The Cambridge Crystallographic Data Centre, 12 Union Road, Cambridge CB2 1EZ, UK; fax: +44(0)1223-336033.

REFERENCES

1. Venkata, S.R.G.; Narkhede, U.C.; Jadhav, V.D.; Gangu, N.; Bobde, Y.;Ghosh, B. Design, synthesis and anticancer evaluation of spiro [cyclohexane-1,1′-indene]-2,5-diene analogues. *ChemistrySelect* **2018**, 3, 12139-12143.
2. Chen, C.; He, L. Advances in research of spirodienone and its derivatives: Biological activities and synthesis methods. *Eur. J. Med. Chem*. **2020**, 203, 112577.
3. Pinto, O.; Sardinha, J.; Vaz, P.D.; Piedade, F.; Calhorda, M.J.; Abramovitch, R.; Nazareth, N.; Pinto, M.; Nascimento, M.S.J.; Rauter, A.P. Synthesis of tetrahydronaphthalene lignan esters by intramolecular cyclization of ethyl p-azidophenyl-2-phenylalkanoates and evaluation of the growth inhibition of human tumor cell lines. *J. Med. Chem*. **2011**, 54, 3175-3187.
4. Nicolaou, K.C.; Kang, Q.; Wu, T.R.; Lim, C.S.; Chen, D.Y.K. Total synthesis and biological evaluation of the resveratrol-derived polyphenol natural products hopeanol and hopeahainol A. *J. Am. Chem. Soc*. **2010**, 132, 7540-7548.
5. Wang, P.; Liu, F.; Zhong, Q.; Zheng, S.L.; Chen, Y.; Wang, G.D.; He, L. Chemoselective synthesis and cytotoxic activity of a series of novel benzo[1,4]oxazin-3-one derivatives. *Chin. Chem. Lett*. **2017**, 1243-1247.
6. Li, Y.H.; Li, H.M.; He, J.; Deng, X.; Peng, L.Y.; Gao, L.H.; Zhao, Q.S.; Li, R.T.; Wu, X.D. (±)-Evodiakine, A pair of rearranged rutaecarpine-type alkaloids from *Evodia rutaecarpa*. *Tetrahedron* **2014**, 70, 8893-8899.
7. Lai, Y.; Liu, T.; Sa, R.; Wei, X.; Xue, Y.; Wu, Z.; Luo, Z.; Xiang, M.; Zhang, Y.; Yao, G. Neolignans with a rare 2-oxaspiro[4.5]deca-6,9-dien-8-one motif from the stem bark of *Cinnamomum subavenium*. *J. Nat. Prod*. **2015**, 78, 1740-1744.
8. Granica, S.; Piwowarski, J.P.; Randazzo, A.; Schneider, P.; Zyzynska-Granica, B.; Zidorn, C. Novel stilbenoids, including cannabispiradienone glycosides, from Tragopogon tommasinii (Asteraceae, Cichorieae) and their potential antiinflammatory activity. *Phytochemistry* **2015**, 117, 254-266.
9. Bondar, D.; Karpichev, Y. Poly(ADP-Ribose) polymerase (PARP) inhibitors for cancer therapy: Advances, challenges, and future directions. *Biomolecules* **2024**, 14, 1269.
10. Feng, Y.; Wang, L.; Niu, S.; Li, L.; Si, Y.; Liu, X.; Che, Y. Naphthalenones from a Perenniporia sp. inhabiting the larva of a phytophagous weevil, euops chinesis. *J. Nat. Prod*. **2012**, 75, 1339-1345.
11. Wang, X.; Wang, M.; Zhang, Z.; Wei, D.; Cai, S.; Li, Y.; Zhang, R.; Zhang, L.; Zhang, R.; Zhu, C.; Huang, X.; Gao, F.; Gao, P.; Wang, Y.; and Huang, W. De Novo design of spiro-type hole-transporting material: Anisotropic regulation toward efficient and stable perovskite solar cells. *Research* **2024**, 7, 0332.
12. Yu, H.J.; Xiao, J.; Chen, J.; Ren, X.; Qi, Y.E.; Min, X.; Shao, G. Synthesis, properties, and application of small-molecule hole-transporting materials based on acetylene-linked thiophene core. *Molecules* **2023**, 28, 3739.
13. Luo, X.; Boschloo, G.; Kloo, L.; Sun, L.; Bo Xu, B. Spiro[fluorene-9,9′-xanthene]-based hole-transporting materials for photovoltaics: Molecular design, structure–property relationship, and applications. *Acc. Mater. Res*. **2024**, 5, 220-235.
14. Shariatinia, Z. Designing novel spiro compounds as favorable hole transport materials for quantum dot sensitized photovoltaics. *Solar Energy* **2022**, 236, 548-560.

15. Abdelali, S.; Idrissi, A.; Tofaïl, I.; Zouhair, E.F.; Said, B. Recent advances in spiro-OMeTAD, thiophene and ethylenedioxythiophene-based hole transport materials for perovskite solar cells: A review. *Mater. Today Energy* **2025**, 51, 101912.
16. Panda, S.S.; Jain, S.C. On water synthesis of spiro-indoles via Schiff bases. *Monatsh Chem.* **2012**, 143, 1187-1194
17. Arya, K.; Rawat, D.S.; Dandia, A.; Sasai, H. Brønsted acidic ionic liquids: Green, efficient and reusable catalyst for synthesis of fluorinated spiro [indole- thiazinones/thiazolidinones] as antihistamic agents. *J. Fluorine Chem*. **2012**, 137, 117-122.
18. Pandey, M.; Raghuvanshi, D.S.; Singh, K.N. Microwave-assisted, solventfree synthesis of 3 -(aryl/heteroaryl)-1-morpholinomethyl/piperidinomethylspiro[3H-indole-3,2 -thiazolidine]-2,4 (1H)-diones via 3-Isatinimines. *J. Heterocycl. Chem*. **2009**, 46, 49-53.
19. Engen, K.; Sa vmarker, J.; Rosenstro m, U.; Wannberg, J.; Lundba ck, T.; Jenmalm-Jensen, A.; Larhed, M. Microwave heated flow synthesis of spiro-oxindole dihydroquinazolinone based IRAP inhibitors. *Org. Pro. Res Dev*. **2014**, 18, 1582-1588.
20. Sachdeva, H.; Saroj, R.; Dwivedi, D. Nano-ZnO catalyzed multicomponent one-pot synthesis of novel spiro(indoline-pyranodioxine) derivative. *Sci. World J.* **2014**, 2014, 427195.
21. Akkurt, M.; Cihan-Ustundag, G.; Capan, G.; Turktekin-Celikesira S.; Tahir, M.N.5-Chloro-4'-ethyl-3H-spiro[1,3-benzothiazole-2,1'cyclohexane], *Acta Cryst*. **2012**, E68, o1466
22. APEX2, SADABS and SAINT Bruker AXS Inc: Madison, WI, USA (2010).
23. Sheldrick G.M. SHELXT-integrated space-group and crystal-structure determination. *Acta Cryst A* **2015**, 71, 3-8.
24. Sheldrick, G.M. Crystal structure refinement with SHELXL. *Acta Cryst* C. **2015**, 71, 3–8.
25. Hübschle, C.B.; Sheldrick, G.M.; Dittrich, B. ShelXle: A Qt Graphical user interface for SHELXL. *J. Appl. Cryst*. **2011**, 44, 1281-1284.
26. Farrugia, L.J. ORTEP-3 for Windows - a version of ORTEP-III with a Graphical User Interface (GUI). *J Appl Cryst.* **1997**, 30, 565.
27. Macrae, C.F.; Bruno, I.J.; Chisholm, J.A.; ENdgington, P.R.; McCabe, P.; Pidcock, E.; Rodriguez-Monge, L.; Taylor, R.; van de Streek, J.; Wood, P.A. New features for the visualization and investigation of crystal structures. *J. Appl. Cryst.*, **2008**, 41, 466-470.
28. Spek. A.L. Structure validation in chemical crystallography. *Acta Cryst*. D **2009**, 65, 148-155.
29. Frisch, M.J.; Trucks, G.W.; Schlegel, H.B.; Scuseria, G.E.; Robb, M.A.; Cheeseman, J.R.; Montgomery, J.A.; Vreven, T.; Kudin, K.N.; Burant, J.C.; Millam, J.M.; Iyengar, S.S.; Tomasi, J.; Barone, V.; Mennucci, B.; Cossi, M.; Scalmani, G.; Rega, N.; Petersson, G.A.; Nakatsuji, H.; Hada, M.; Ehara, M.; Toyota, K.; Fukuda, R.; Hasegawa, J.; Ishida, M.; Nakajima, T.; Honda, Y.; Kitao, O.; Nakai, H.; Klene, M.; Li, X.; Knox, J.E.; Hratchian, H.P.; Cross, J.B.; Adamo, C.; Jaramillo, J.; Gomperts, R.; Stratmann, R.E.; Yazyev, O.; Austin, A.J.; Cammi, R.; Pomelli, C.; Ochterski, J.W.; Ayala, P.Y.; Morokuma, K.; Voth, G.A.; Salvador, P.; Dannenberg, J.J.; Zakrzewski, V.G.; Dapprich, S.; Daniels, A.D.; Strain, M.C.; Farkas, O.; Malick, D.K.; Rabuck, A.D.; Raghavachari, K.; Foresman, J.B.; Ortiz, J.V.; Cui, Q.; Baboul, A.G.; Clifford, S.; Cioslowski, J.; Stefanov, B.B.; Liu, G.; Liashenko, A.; Piskorz, P.; Komaromi, I.; Martin, R.L.; Fox, D.J.; Keith, T.; Al-Laham, M.A.; Peng, C.Y.; Nanayakkara, A.; Challacombe, M.; Gill, P.M.W.; Johnson, B.; Chen, W.; Wong, M.W.; Gonzalez, C.; Pople J. A. Gaussian 09, Revision A.02, Gaussian, Inc., Wallingford CT, **2016**.
30. Yanai, T.; Tew, D.P.; Handy, N.C. A new hybrid exchange–correlation functional using the Coulomb-attenuating method (CAM-B3LYP). *Chem. Phys. Lett*. **2004**, 393, 51-57.
31. Salavati-Niasari, M.; Mirsattari, S.N.; Monajjemi, M.; Hamadanian, M. Density functional B3LYP and B3PW91 studies of the properties of four cyclic organodiboranes with

tetramethylene fragments. *J. Struct. Chem.* **2010**, 51, 437-443.
32. Chai, J.D.; Head-Gordon, M. Long-range corrected hybrid density functionals with damped atom–atom dispersion corrections. *Phys. Chem. Chem. Phys*. **2008**, 10, 6615-6620.
33. GaussView, Version 6, Dennington, Roy; Keith, Todd A.; Millam, John M. Semichem Inc., Shawnee Mission, KS, **2016**.
34. M. D. Hanwell, D. E. Curtis, D. C. Lonie, T. Vandermeersch, E. Zurek and G. R. Hutchison, Avogadro: An advanced semantic chemical editor, visualization, and analysis platform. *J. Cheminform*. **2012**, 4, 17.
35. Spackman, P.R.; Turner, M.J.; McKinnon, J.J.; Wolff, S.K.; Grimwood, D.J.; Jayatilaka, D.; Spackman, M.A. CrystalExplorer: a program for Hirshfeld surface analysis, visualization and quantitative analysis of molecular crystals. *J. Appl. Cryst*. **2021**, 54, 1006-1011.
36. Guin, M.; Khanna, S.; Elavarasi, S.B.; Sarkar, P. DFT calculations, Hirshfeld surface analysis and docking studies of 3-anisaldehyde thiosemicarbazone, *J. Chem. Sci*. **2020**, 132, 1-11.
37. Lahmidi, S.; Bakheit, A.H.; Essassi, E.M.; Mague, J.T.; Alanazi, M.M.; X-ray crystal structure, Hirshfeld surface analysis, DFT, and anticancer effect of 3-hydroxy-4-phenyl-1,5-benzodiazepin-2-one derivatives. *Crystals* **2023**, 13, 1-18.
38. Elleuch, N.; Fredj, D.; Chniba-Boudjada, N.; Boujelbene, M. Synthesis of a new chloro antimony complex with pyridinium derivative: Crystal structure, Hirshfeld surface analysis, vibrational, and optical properties. *J. Inorg. Organomet. Polym.* **2020**, 30, 889-898.
39. Choi, C.H.; Kertez, M. Conformational information from vibrational spectra of styrene, trans-stilbene, and cis-stilbene. *J. Phys. Chem*. *A* **1997**, 101, 3823-3831.
40. Kurt, M.; Chinna Babu, P.; Sundaraganesan, N.; Cinar, M.; Karabacak, M. Molecular structure, vibrational, UV and NBO analysis of 4-chloro-7-nitrobenzofurazan by DFT calculations. *Spectrochim Acta A* **2011**, 79, 1162-1170.
41. Lewis, D.F.V.; Ioannides, CDV. Interaction of a series of nitriles with the alcohol-inducible isoform of P450: Computer analysis of structure—activity relationships *Xenobiotica* **1994**, 24, 401-408.
42. Padmaja, L.; Kunar, R.C.; Sajan, D.; Joe, I.H.; Jayakunmar, V.S.; Pettit, G.R.; Nielsen, O.F. Density functional study on the structural conformations and intramolecular charge transfer from the vibrational spectra of the anticancer drug combretastatin-A2. *J. Raman Spectrosc*. **2009**, 40, 419-428.
43. Poiyamozhi, A.; Sundaraganesan, N.; Karabacak, M.; Tanriverdi, O.; Kurt. M. The spectroscopic (FTIR, FT-Raman, UV and NMR), first-order hyperpolarizability and HOMO–LUMO analysis of 4-amino-5-chloro-2-methoxybenzoic acid. *J. Mol. Struc*. **2012**, 1024, 1-12.
44. Udhayakala, P.; Jayanthi, A.; Rajendiran, T.V.; Gunasekaran, S. Molecular structure, FT-IR and FT-Raman spectra and HOMO-LUMO analysis of 2-methoxy-4-nitroaniline using ab initio HF and DFT (B3LYP/B3PW91) calculations. *Arch. Appl. Sci. Res.* **2011**, 3, 424-439.
45. Sucharitha, P.; Ramesh Reddy, K.; Satyanarayana, S.V.; Garg, T. Chapter 15 - Absorption, distribution, metabolism, excretion, and toxicity assessment of drugs using computational tools, *Computational Approaches for Novel Therapeutic and Diagnostic Designing to Mitigate SARS-CoV-2 Infection Revolutionary Strategies to Combat Pandemics* **2022**, 335-355.
46. Kola, I.; Landis, J. Can the pharmaceutical industry reduce attrition rates? *Nat. Rev. Drug Discov*. **2004**, 3, 711-715.
47. Keller, T.H.; Pichota, A.; Yin, Z. A practical view of 'druggability'. *Curr. Opin. Chem. Biol*. **2006**, 10, 357-361.
48. Ursu, O.; Rayan, A.; Goldblum, A.; Oprea, T.I. Understanding drug-likeness. *Wiley Interdiscip. Rev. Comput. Mol. Sci*. **2011**, 1, 760-781.

49. Odame, F.; Hosten, E.C.; Betz, R.; Lobb, K.; Tshentu Z.R. Characterization and Computational Studies of 2-(Benzamido)Thiazol-5-yl Benzoate, *J. Struc. Chem*. **2019** 60, 136-142.
50. Odame, F.; Krause, F.; Hosten, E.C.; Betz, R.; Lobb, K.; Tshentu, Z.R.; Carminita L. Frost, Synthesis, characterization and DPPH scavenging activity of some benzimidazole derivatives. *Bull. Chem. Soc. Ethiop.* **2018**, 32, 271-284.